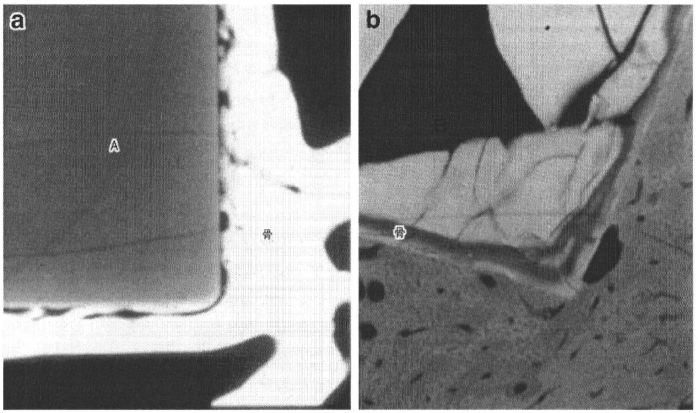

図1　骨にインプラントした8週目のアルミナセラミックスとBioglassのCMR像
アルミナでは材料と骨の間で間隙があるがBioglassでは骨が材料に直接つながり間隙はない．Bioglassの親和性の高さが認められる．
a：Alumina．b：Bioglass
（整形外科セラミックインプラントコロキュウム記録集 1巻．1980，p69-72）

いられるようになるには電子材料や原子炉材料のためのファインセラミックスが開発され実用化されたのち，1960年以降である．

セラミックスは焼結して作製した非金属の無機固体材料の総称である．金属が常にイオンの溶出が問題となるのに対して，セラミックスはアルミナに代表されるように安定で，溶出などの心配がなく金属に代わる生体材料として期待された[2]．アルミナは，スクリューやピンなどの骨接合材として開発され，つぎに，骨補填材料としても臨床応用された．しかし，アルミナやジルコニアなどのセラミックスは金属や骨にくらべ破壊靭性が低く，硬度が高いために加工性に問題があり，骨接合材や骨補填材料としては発展せず，現在はその耐摩耗性から人工関節の摺動部材料として発展している．一方，セラミックのなかでも骨の無機成分であるリン酸カルシウムは骨補填材料として骨置換や骨接合に効果を期待され，Albee（イギリス）らはリン酸カルシウム化合物を脊椎の後方固定に用いたと報告している．その後，ファインセラミックの技術を応用して骨の無機成分結晶と同じ水酸アパタイト（HA）の合成が研究され，日本の青木ら[3]やアメリカのJarchoら[4]により実用化され臨床応用されている．

1969年，HAが実用化されたころに，ガラスの研究者であったアメリカのHenchがにリン酸カルシウムを含むガラスが骨と化学的に結合することを見いだし，これをBioglassと称した[5]．HAにも同様に骨と化学的に結合する性質が見いだされ，従来のアルミナやジルコニアは化学的安定性からbioinert ceramics，骨と結合できるBioglassやHAはbioactive ceramicsと分類されている（図1）．骨補填材料としてはbioactive ceramicsがすぐれており，HAやガラスセラミックを用いた多くの骨補填材料が開発された．その後はセラミックスの焼結温度や組成を変化させて強度を高くする試みや，内部まで細胞や血管が侵入できるように連通孔を持たせる多孔化の研究が進められた．

骨にあるリン酸カルシウム結晶はHA以外の組成を多く含んでいる．そのなかで，生体内で吸収されやすい性質を持つ組成を選んでセラミックスを合成することで，生体吸収性の骨置換材料の開発が行われ，三リン酸カルシウム（TCP）として実用化されている．また，リン酸カルシウムは組成により，その紛体表面にHAを形成して固化するというセメント

表1　自家骨移植(腸骨採取)の合併症

Major(8.6%)	感染(2.5%) 創遷延治癒(0.8%) 大きな血腫(3.3%) 再手術(3.8%) 6カ月以上つづく疼痛(2.5%) 知覚障害(1.2%) 醜状瘢痕
Minor(20.6%)	表層感染，minorな創の問題，一過性の知覚障害，一過性の疼痛

(Younger EM et al.: J Orthop Trauma　1989, 3:192-195)

様の性質を持つことから，リン酸カルシウム骨セメントとして臨床応用されている．

高分子材料は1920年代に多数の材料が合成され，現在はプラスチックの時代といわれるほどの隆盛を極めている．これらの材料は生体材料としても，縫合糸などの手術材料全般において，金属やガラス製品に置き換わって使用されることとなっている．整形外科分野では，縫合材や創を被覆する材料を除くと，骨置換や関節置換材料として用いられているPMMA骨セメントと超高分子ポリエチレンが重要である．

骨セメントは歯科材料から整形外科領域に応用されたものであるが，超高分子ポリエチレンとともに人工関節の実用化に不可欠な材料であった．骨セメントは人工関節の固定だけでなく，骨粗鬆症や転移性腫瘍による脊椎圧迫骨折部に充填することで骨補填材料としても使用されている．また，高分子材料のなかでもポリグリコール酸やポリ乳酸は吸収性材料として開発され，骨固定用のスクリューやプレートなどとして実用化されている．これらの材料は生体活性セラミックスなどとの複合化により生体活性を賦与したり，多孔化によって骨補填材料としての機能を高めたりする研究も進められ成果を上げている．これらの吸収性多孔性生体活性材料は骨補填材料としてのみならず，再生医学の分野におけるスカフォールドとしての応用も見込まれている．

骨再建用人工材料に求められる特性

外傷や腫瘍，感染，変性疾患などの疾病とそれによる運動器機能やQOLの低下をきたす患者は依然増加しており，運動器再建手術の果たす役割は高まっている．そのような運動器再建手術においては荷重に対する支持機能の再建を要することが多い．具体的には，腫瘍や感染，人工関節のゆるみなどにより生じた骨欠損のため骨が支持機能を失った場合や，骨折などの場合である．骨欠損を骨補填材料を用いて補っても，即時的には充分な支持機能を獲得できない場合も多く，そのような場合には骨接合術と同様に内固定材を用いた固定術が併用される．そのような骨接合材料については骨補填材料と違い，生体活性よりも強度や操作性などが優先される．

一方，骨補填材として通常は自家骨が用いられることが多く，依然骨補填材としての第1選択となっている[6]．しかし，採取できる自家骨量には限界があり，自家骨採取に際して健常部に侵襲を加えることが必要であるため，表1のようにさまざまな合併症も報告されている．一方で，心臓死のドナーから採取したり，手術で余った骨を保存したりして使用する同種骨も骨補填材として使用されている．

骨は97%が骨基質で，骨髄細胞を除くと抗原性を生む細胞成分が少なく，さらに，骨組織中には骨誘導因子やその他の成長因子が含まれており，これらは骨増殖や骨分化を促進するものである．同種骨はそのような生物学的活性では自家骨に劣るものの人工骨よりはすぐれており，量の制限がないため，欧米では一般的な方法である．しかし，同種骨は心臓死のドナーから採取し，凍結保存して使用する必要があり，社会的な合意と骨銀行の整備が必要である．わが国では骨銀行は一部の地域を除き充分整備されていないのが現状である．また，感染症の伝搬を生じる可能性もゼロではない．以上の理由により，大きな骨欠損の補填や，自家骨採取による侵襲を避けるために，すぐれた骨補填材料の開発が期待されることになる．

このように，骨再建用生体材料として求められる特性は，その用途により異なり，主に支持機能を再建することを目的とするものと，骨補填材としての機能を目的とするものに分類されるが，両者を併せ持つ材料もあり，厳密な分類ではない．

1. 支持機能を再建するために必要とされるマテリアルの特性

支持機能を主眼としたマテリアルには，材料そのものが充分な支持機能を有するものや，材料そのものの支持機能は不十分であっても，骨折部や骨欠損部の骨形成により最終的には正常骨としての支持機能を獲得できるものなどがある．前者の例としては人工関節や人工椎体が，後者の例としては骨接合材や脊椎固定用インプラントなどがあげられる．これらのデバイスには，その高い力学的信頼性から金属材料が使用されることが多い．人工関節など，即時に荷重支持機能が獲得される手術においては，材料は患者の体内にほぼ一生涯埋入されることになるため，材料そのものに充分な支持機能が要求されるだけでなく，次項で述べるような骨補填材としての機能も高いレベルで要求される．

骨接合材などでは，手術後即時に荷重支持機能が獲得されることが望ましいが，手術後には完全な支持機能が得られなくとも，骨癒合までの一定期間破綻をきたさない程度の強度があれば術後免荷や外固定などの後療法によって対応できるため使用可能である．骨接合材は骨癒合が得られ，その支持機能が必要なくなると抜去可能となる．したがって，材料それ自身は骨補填材のように骨と直接結合する機能はないほうがよい．ポリ乳酸などからなる吸収性骨接合材であれば抜去の必要はなくなるが，吸収性，強度，生体親和性などの各要素が高レベルで最適化されていなければならない．

四肢，骨盤，脊椎などのいずれの骨であれ荷重を支える必要があるが，その程度は，部位や生活動作によって当然違いがある．たとえば，大腿骨頭には片脚起立時に体重の3倍の荷重が掛かり，走ったり階段上昇したりする際には4～5倍の荷重が掛かると考えられている[7]．

2. 骨補填材として必要とされるマテリアル特性

骨補填材として要求される特性は，高い骨組織親和性と骨組織としての構造を維持するための充分な強度を両立していることである．一般に骨補填材とは，人工骨として患者の体内に埋入され骨としての機能を代替させるものであるが，骨組織親和性が高いものでは骨組織同様にリモデリングを受け，その強度は必要に応じて経時的に高まることがわかっている．そのため，骨補填材としての機能を高める際には，多孔化などにより強度を犠牲にしても骨親和性を高めることが優先される傾向にある．

生体材料は生体中では基本的には被膜に覆われる．材料の組織親和性は被膜の厚さに反比例するといわれている[8]．しかし，骨補填材料として骨親和性がすぐれたものは軟組織を介さず直接に骨組織と接触し，骨と結合することが出来ることがわかっている．このことは，骨が軟組織を介さずに直接に生体材料に荷重を伝達できることになり，周囲の骨組織からのリモデリングを受けることで強度が必要に応じて高まることに直結するため，骨補填材として必須の機能である．非吸収性材料では特にこの界面性状が重要である．材料が吸収され骨に置換される材料では，界面の問題は少なくなるが，一般に強度が低いことや，材料の吸収と骨形成のバランスの問題がある．したがって，TCPに代表される吸収性骨補填材は，前項で述べたように骨接合材を併用して支持機能を補ったり，慎重な後療法を行ったり，荷重の少ない部位で使用するなどの注意が必要となる．

骨欠損は三次元的な構造を持っている．この欠損の形状に合わせ骨補填材料はさまざまな形態で用いられる．欠損部が骨に取り囲まれている構造であれば，顆粒状の骨補填材をパッキングすることで補うことが出来る．しかし，欠損が大きく，骨補填材料で骨の外形も形成する必要がある場合には顆粒などでは補填できず，材料そのものが骨の欠損に合わせた形態を有する必要がる．現在の骨の補填材料は既成品としてつくられており，金属やセラミックスは欠損に応じて術中に加工することは困難である．骨セメントのようにその場で形成し，固化して自由な構造が出来るものもあるが，PMMA骨セメントは骨親和性の点で不十分であり，リン酸カルシウム骨セメントは，大きな骨欠損を充分な強度をもって補填するには不十分である．

3. 骨再建用人工材料に求められるその他の特性

手術用材料である以上，材料の滅菌性は重要であり，オートクレーブ滅菌，エチレンオキサイドガス

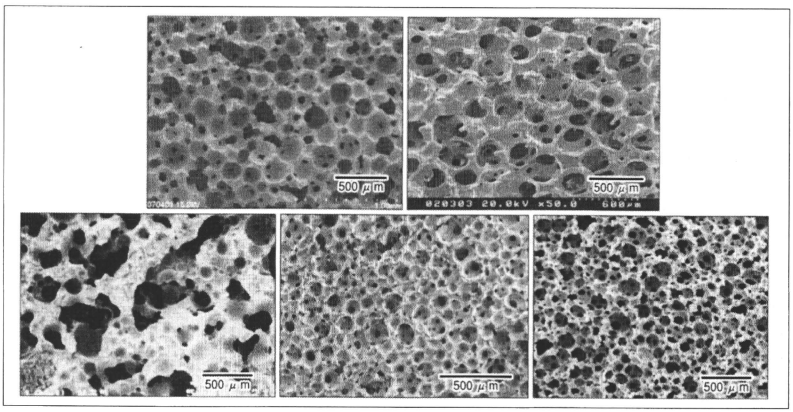

図2　各種人工骨用セラミックス多孔体のSEM像
70%を超える気孔率では連通孔がみられるが，材料によってサイズや形態がかなり異なっている．
a：AWGCビーズ法(気孔率80%)．b：AWGCスポンジ法(気孔率70%)．c：オスフェリオン(75%)
d：NEOBONE(気孔率72～78%)．e：アパセラム-AX(気孔率85%)　　(メーカーカタログより)

表2　高気孔率多孔性生体活性セラミックス材料

	オスフェリオン*1)	ネオボーン*2)	アパセラム-AX*3)
材　料	β-TCP	HA	HA
気孔率	75%	75%	85%
気孔径(μm)	100～400	150	200
連通気孔(μm)	-	10～50	50～100
圧縮強度(MPa)	0.9	12	0.7

*1) オリンパステルモバイオマテリアル社．*2) コバレントマテリアル社．*3) ペンタックス社

滅菌，ガンマ線照射滅菌などの各種滅菌法に対し，材料の性質が変わることなく滅菌可能でなければならない．また，近年の医療の現場ではMRIやCT撮像は診断上必須の項目となってきており，それらの撮影に障害がなくかつ画像に影響を与えないものがよい．MRI，CT耐性という点においては，金属材料は他の材料に劣る．

運動器再建材料の現況と展望

1．金属材料

金属材料は一般に，金属結合により構成される多結晶体を指す．バイオマテリアルとして使用する際の金属材料は，強度や破壊靱性にすぐれるため荷重部であっても使用可能である[9]．短所としては，腐食によって溶出した金属イオンやその誘導体である酸化物や水酸化物，あるいは金属磨耗粉などが生体毒性を示す可能性があること，腐食および疲労によりインプラントの破壊を起こすおそれがあることなどである．しかし，金属材料はその高い力学的信頼性から，骨接合材，脊椎固定用インプラント，人工椎体，人工関節など大きな荷重が掛かる部位において，依然として多くのデバイスに使用されている．

金属系バイオマテリアルの多くはステンレス鋼，コバルトクロム合金など一般に使用されてきた材料を医療用へ転用したものがほとんどであるため，ニッケル(Ni)やバナジウム(V)，アルミニウム(Al)など生体に好ましくない構成元素を有しているという問題点がある[10]．そのため，生体為害性元素を含まない生体用金属材料の開発が進められている．ステ

ンレス鋼においては金属アレルギー感作率の高いNiを含まない生体用ステンレス鋼の開発が，チタン合金では現在無毒性元素として考えられているTi，ニオブ(Nb)，タンタル(Ta)およびジルコニウム(Zr)を構成元素とするチタン合金の開発[11,12]が進められている．生体無毒性元素からなる金属材料では低弾性や形状記憶性などの従来のチタン合金にはなかった新たな機能を付与する試みも行われている[12,13]．

金属材料のなかでも，チタンおよびその合金は軽量で高い破壊靱性を示し，他の金属にくらべ生体親和性の点ですぐれているので，広く臨床応用されている．しかし，チタン金属は高い生体親和性を示すものの，そのままでは骨と直接結合することはない．表面をチタンのプラズマ照射やファイバーやビーズの溶接による多孔体表面にして骨の侵入を得るか，HAコーティング[14]や表面の化学処理による表面金属の生体活性化により骨との結合性を付加することが出来る．界面の長期安定化には表面の多孔化と生体活性化を組み合わせ，多孔化表面に生体活性化[15~17]が行われる．多孔構造の粗面を活かすにはHAなどのプラズマ溶射よりアルカリ加熱処理による表面化学処理が有利と考えられる．

近年，生体材料の分野ではさまざまな多孔構造を持つ多孔性生体材料の開発が盛んである．金属材料においても，多孔化により組織侵入による機械的結合が得られるため骨移植を省略出来ること，弾性率を低下させてストレスシールディングを予防できることといった効果が期待できる．すでに欧米においてはTa[18]などの多孔体の臨床応用が開始されている．筆者もアルカリ加熱処理多孔体チタンの臨床応用を進めており，生体活性化処理により骨伝導能[19]だけでなく骨誘導能[20]を有する新世代の金属性インプラントとして期待されてる[21]．

2. セラミックス

前述のようにセラミックス材料として，アルミナやジルコニアなどのbioinert ceramicsと，Bioglass，HAなどのbioactive ceramicsがあるが，後者のほうが骨置換材料としては適している．骨の無機成分であるHAは骨置換材料としては基本となっている．HAは焼結した緻密体では皮質骨に匹敵する強度が得られている．また，**図2**や**表2**に示されるように気孔形成材を利用して多孔体の作製が可能で，さまざまな気孔率のものが用いられている．多孔体では100 μm以上の気孔径を有する気孔が骨組織の形成に有利と考えられている．さらに中心部まで骨組織が進入するには連通孔としてつながっている必要があり，その連通孔の径も数十μm以上の大きさが必要である．

HAは一部のリン酸基をケイ素や亜鉛に変えると骨形成が促進されることが知られており，ケイ素や亜鉛含有水酸アパタイトが開発されている．水酸アパタイトは中性領域では焼結体はほとんど吸収されないが，TCPや炭酸アパタイトは中性領域でも溶解することが知られており，これらの焼結体が開発されている．このなかでTCPはすでに多孔体や焼結体が吸収性材料として市販されている．TCPの吸収は溶出のみでなく，破骨細胞が吸収に寄与していることが判明しており，骨のリモデリングの機序に類似した形で置換が行われると考えられる[22]．

Bioglassは人工骨として骨形成や骨結合性にすぐれているがわが国では市販されていない．高強度，高生体活性を両立したセラミックス材料として結晶化ガラスAW(AW-GC)[23,24]が京都大学のグループによって開発され，荷重部でも使用可能なセラミックス材料として臨床応用されたが，現在は販売中止となっている．また，体内で徐々に硬化する粘土状あるいはペースト状のリン酸カルシウム系硬化型骨補填材(calcium phosphate cement: CPC)なども使用可能となっており，臨床の場では使用する状況・病態・目的に応じて使いわけられている．

これらの生体活性セラミックス材料に対して，アルミナ(Al_2O_3)やジルコニア(ZrO_2)などは生体内では異物反応をほとんど示さない生体不活性(bioinert)な性質を持ち，その高い耐摩耗性のために主に人工関節の摺動面として用いられている．アルミナは機械的強度や硬度にすぐれているだけでなく，耐腐食性にもすぐれている．しかしながら破壊靱性が低く，脆弱性があるため破損の危険性があり，インプラントのデザインや手術手技上の制限がある．一方で，ジルコニアは破壊靱性や曲げ強度などの機械的特性にすぐれるため，現在の人工関節の摺動面に使用さ

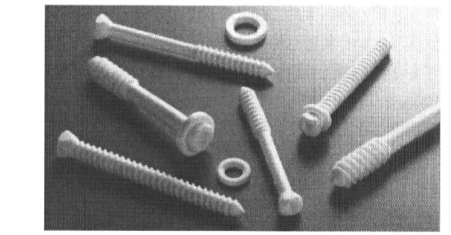

図3　ポリ乳酸と焼結アパタイトの複合材からつくった骨固定用の螺子
ポリ乳酸の材料にくらべ，吸収後に骨形成が良好である．

れるセラミックス材料の主流となっている[25]．しかし，ジルコニアには生体内で正方晶から単斜晶へ相転移を起こし劣化するいわゆる低温劣化の問題があり，長期の安定性や耐摩耗性については議論の余地がある[25]．このような状況から，近年の人工関節摺動面用のセラミックス材料は耐摩耗性だけでなく，高強度，高破壊靱性，高安定性をキーワードとして開発が進められている．アルミナ，ジルコニアをベースに強化したジルコニア強化アルミナ(zirconia toughened alumina: ZTA)やアルミナ強化ジルコニア(alumina toughened zirconia: ATZ)といった複合材料はその一例である．このようなアルミナ/ジルコニア複合材料はすでに欧米では臨床応用が開始されており[26]，日本でもまもなく販売開始される予定がある(JMM社，personal communicationによる)．

3．高分子材料

高分子材料は金属，セラミックス材料と並んで整形外科分野で重要な役割を示す材料の一つである．高分子(ポリマー)材料とは多数の低分子(モノマー)が共有結合で連なることで形成される，分子量がほぼ1万以上の材料を指す．モノマーの種類や連なり方によってさまざまな性質を持つため医療分野においてもPMMA骨セメント，吸収性骨置換材料，人工股関節摺動面用のポリエチレンなどさまざまな高分子材料が運動器再建に使用されている．

PMMA骨セメントは骨補填材料として使用されている．PMMA骨セメントは親和性では生体活性材料にくらべ劣るものの，強度と操作性において補填材料としてすぐれた材料である．PMMA骨セメントが生体材料として使用されるようになって40年以上が経過しているが，メチルメタアクリレートの液とポリメチルメタアクリレートの粉末を混合して，ダフフェーズを経て硬化させるという基本的な点はほとんど変わっていない．そのため，組織親和性に関しては大きな改良がなされていないのが現状であり，強度と骨親和性にすぐれた骨セメントの開発が期待されている．

合成高分子の吸収性材料としてはポリグリコール酸とポリ乳酸が用いられている．骨ではすでに螺子としてポリ乳酸が使用されているが，強度の低下にくらべ，材料が吸収されてなくなるまでに，期待されていたよりも長期間を要することがわかっており，骨の再生が遅れる傾向も認めたため，水酸アパタイトとの複合材が開発され親和性が向上したものが市販されている[27](図3)．この材料は多孔体にすることも可能で，吸収性材料としての応用も可能である[28]．また，骨基質と同様にコラーゲンと水酸化アパタイトを混合したものが市販されていたが，四宮らはナノ結晶の水酸アパタイトとアテロコラーゲンとの複合材料を開発し[29]，荷重の比較的掛からない部位での骨置換材料としてTCPとの比較臨床治験を進めている．いずれの材料もアパタイトと有機材料の複合化材料であり，破骨細胞を介しての吸収が認められ，骨リモデリングの機序で骨再生が行われるものと考えられる．これらの材料は使用部位が限定されるが，細胞を用いた骨再生医療のスカフォールドとしての応用も期待される．

骨置換材料の作成法の改善と新手法の開発

三次元積層法

金属やセラミックスは基本的に高温による焼結によって作製される．通常は鋳型に入れて焼結されるが，それに代わる造形法としてインクジェット方式による三次元積層造形法または選択的レーザー溶融(http://lasersintering.com/)[30]や電子ビーム技術を利用した金属積層造形法がTCPやチタン金属に応用され，CT画像に基づき三次元的な造形が高精度に可能となってきた(http://www.arcam.com/)[31](図4)．

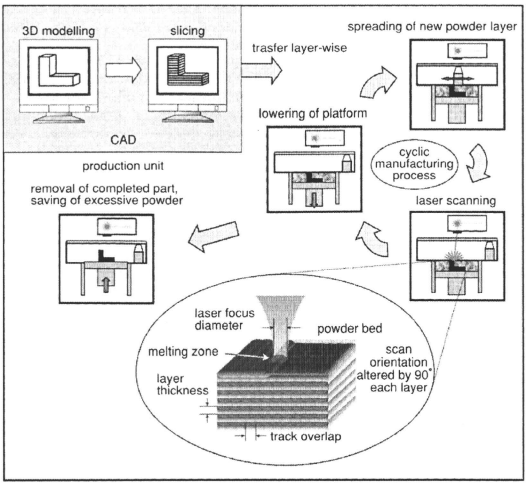

図4
レーザー選択的焼結による三次元積層造形法の模式図
この方法により，CTなどで得られた画像データから任意の形状のチタン金属がつくり出せる．
(Hollander DA et al., 2006)[31]

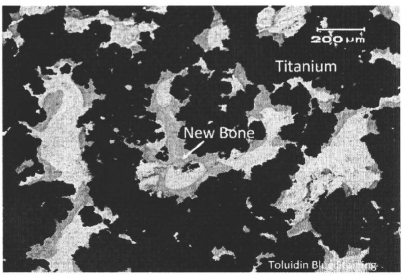

図5　12カ月のbioactiveポーラスチタン
黒くみえるチタンでつくられたポーラス体内部にトルイジンブルーでよく染まる旺盛な骨形成が観察される
(Fujibayashi S et al., 2004)[20]

これらの方法は患者の骨欠損の形状に三次元的に適合する人工骨を提供する方法であり，テーラーメード医療を可能にする[32]．生体材料の開発はこのようなプロセスの改良によっても大きく進歩することが期待される．

生体材料による骨誘導－構造が生む新しい可能性－

骨内にインプラントを埋入すると生体活性材料では骨組織は材料表面に沿って形成される．また多孔体では，骨内に埋入すると孔のなかに骨組織が進入し，形成される．このような骨組織の成長を骨伝導とよぶ．一方，骨組織を塩酸で脱灰した骨基質は筋肉内に埋入すると，新しく骨細胞が分化し骨を形成してくる．これが骨誘導という現象である．

後者の骨誘導には骨基質中の骨誘導因子というタンパクが作用して骨が分化してくると考えられている．この性質は骨再建にとって非常に有利な特性であるが，通常のセラミックスや金属，ポリマーを筋肉に入れても骨誘導は生じない．しかし，1991年に南アフリカのRipamontiらがサンゴからつくった多孔体HAがbaboonの背筋内で気孔内に骨が形成することを見いだした[33]．

その後HAのみでなく，生体活性材料であるBioglass，TCP，HA/TCP複合材やHAコーティングを行ったタンタル多孔体などでも同様の現象が生じることが見いだされた．さらにチタン多孔体にアルカリ加熱処理を施したものも同様の骨誘導することがわかってきた[20]．(図5)これらの研究から，多孔体表面のミクロ構造とマクロ多孔構造が生物学的反応に強く影響することが判明し，この性質を制御することでこれまでにない生体親和性の高い骨置換材

料が誕生することが期待される．骨再建材料を考えるうえで，材料のミクロからマクロの構造が生体に及ぼす影響を探索し，開発に活かすことが重要と考えられる．

文　献

1) Mears DC ed. : Materialsand orthopaedic surgery. Baltimore, the Williams & Wilkins, 1979.
2) 川原春幸，山上哲賢，平林正也，幸田洋一，横田順一・他：新型セラミック・インプラント "Bio-ceram" について．歯科展望(別冊)インプラントの臨床　1975, 215 : 207-214.
3) Akao M, Aoki H, Kato K: Mechanical properties of sintered hydroxyapatite for prosthetic applications. Journal of Materials Science　1981, 16 : 809-812.
4) Jarcho M, Kay JF, Gumaer KI, Doremus RH, Drobeck HP: Tissue, cellular and subcellular events at a bone-ceramic hydroxylapatite interface. J Bioeng　1977, 1 : 79-92.
5) Hench LL, Paschall HA: Direct chemical bond of bioactive glass-ceramic materials to bone and muscle. J Biomed Mater Res　1973, 7 : 25-42.
6) Urabe K, Itoman M, Toyama Y, Yanase Y, Iwamoto Y et al.: Current trends in bone grafting and the issue of banked bone allografts based on the fourth nationwide survey of bone grafting status from 2000 to 2004. Journal of Orthopaedic Science(0949-2658)　2007, 12 : 520-525.
7) Hodge WA, Fijan RS, Carlson KL, Burgess RG, Harris WH, Mann RW: Contact pressures in the human hip joint measured *in vivo*. Proc Natl Acad Sci USA　1986, 83 : 2879-2883.
8) Williams DF, Roaf R: Implants in surgery. London, WB Sounders, 1973.
9) 塙　隆夫：金属バイオマテリアルの特徴．バイオマテリアル　2007, 25 : 214-220.
10) Yamamoto A, Kohyama Y, Kuroda D, Hanawa T: Cytocompatibility evaluation of Ni-free stainless steel manufactured by nitrogen adsorption treatment. Materials Science and Engineering C　2004, 24 : 737-743.
11) Davidson JA, Mishra AK, Kovacs P, Poggie RA: New surface-hardened, low-modulus, corrosion-resistant Ti-13Nb-13Zr alloy for total hip arthroplasty. Bio-medical materials and engineering　1994, 4 : 231-243.
12) Niinomi M, Hanawa T: Japanese research and development on metallic biomedical, dental, and healthcare materials. JOM　2005, 57 : 18-24.
13) Saito T, Furuta T, Hwang JH et al.: Multifunctional alloys obtained via a dislocation-free plastic deformation mechanism. Science　2003, 300 : 464-467.
14) Geesink RG: Osteoconductive coatings for total joint arthroplasty. Clinical orthopaedics and related research　2002, 395 : 53-65.
15) Kim HM, Miyaji F, Kokubo T, Nishiguchi S, Nakamura T: Graded surface structure of bioactive titanium prepared by chemical treatment. J Biomed Mater Res　1999, 45 : 100-107.
16) Nishiguchi S, Fujibayashi S, Kim HM, Kokubo T, Nakamura T: Biology of alkali- and heat-treated titanium implants. J Biomed Mater Res A　2003, 67 : 26-35.
17) Nishiguchi S, Nakamura T, Kobayashi M, Kim HM, Miyaji F, Kokubo T: The effect of heat treatment on bone-bonding ability of alkali-treated titanium. Biomaterials　1999, 20 : 491-500.
18) Bobyn JD, Poggie RA, Krygier JJ et al.: Clinical validation of a structural porous tantalum biomaterial for adult reconstruction. J Bone Joint Surg Am　2004, 86-A (Suppl 2) : 123-129.
19) Takemoto M, Fujibayashi S, Neo M, Suzuki J, Kokubo T, Nakamura T: Mechanical properties and osteoconductivity of porous bioactive titanium. Biomaterials　2005, 26 : 6014-6023.
20) Fujibayashi S, Neo M, Kim HM, Kokubo T, Nakamura T: Osteoinduction of porous bioactive titanium metal. Biomaterials　2004, 25 : 443-450.
21) Takemoto M, Fujibayashi S, Neo M et al.: A porous bioactive titanium implant for spinal interbody fusion: an experimental study using a canine model. J Neurosurg Spine　2007, 7 : 435-443.
22) Kondo N, Ogose A, Tokunaga K et al.: Bone formation and resorption of highly purified beta-tricalcium phosphate in the rat femoral condyle. Biomaterials　2005, 26 : 5600-5608.
23) Kokubo T, Shigematsu M, Nagashima Y et al.: Apatite- and wollastonite- containing glass- ceramic for prosthetic application. Bull Inst ChemRes Kyoto Univ　1982, 60 : 260-268.
24) Nakamura T, Yamamuro T, Higashi S, Kokubo T, Itoo S: A new glass-ceramic for bone replacement: evaluation of its bonding to bone tissue. J Biomed Mater　Res 1985, 19 : 685-698.
25) Piconi C, Maccauro G: Zirconia as a ceramic biomaterial. Biomaterials　1999, 20 : 1-25.
26) Pria DP: Evolution and new application of the alumina ceramics in joint replacement. European Journal of Orthopaedic Surgery and Traumatology　2007, 17 : 253-256.
27) Shikinami Y, Okuno M: Bioresorbable devices made of forged composites of hydroxyapatite (HA) particles and poly-L-lactide (PLLA): Part I. Basic characteristics. Biomaterials　1999, 20 : 859-877.
28) Hasegawa S, Tamura J, Neo M et al.: *In vivo* evaluation of a porous hydroxyapatite/poly-DL-lactide composite for use as a bone substitute. J Biomed Mater Res A　2005, 75 : 567-579.
29) Itoh S, Kikuchi M, Koyama Y et al.: Development of a novel biomaterial, hydroxyapatite/collagen (HAp/Col) composite for medical use. Biomed Mater Eng　2005, 15 : 29-41.
30) Fukuda A, Takemoto M, Fujibayashi S et al.: Bone ingrowth into pores of lotus-type bioactive titanium fabricated using rapid prototyping technique. Biooceramics　2009, 22: 269-272.
31) Hollander DA, von Walter TWM, Sellei R, Schmidt-Rohlfing OPB, Erli H: Structural, mechanical and *in vitro* characterization of individually structured Ti-6Al-4V produced by direct laser forming. Biomaterials　2006, 27: 955-963.
32) Hollister SJ: Porous scaffold design for tissue engineering. Nat Mater　2005, 4 : 518-524.
33) Ripamonti U: The morphogenesis of bone in replicas of porous hydroxyapatite obtained from conversion of calcium carbonate exoskeletons of coral. J Bone Joint Surg Am　1991, 73 : 692-703.

Acta Biomaterialia 7 (2011) 1379–1386

Contents lists available at ScienceDirect

Acta Biomaterialia

journal homepage: www.elsevier.com/locate/actabiomat

Bone bonding bioactivity of Ti metal and Ti–Zr–Nb–Ta alloys with Ca ions incorporated on their surfaces by simple chemical and heat treatments

A. Fukuda [a,*], M. Takemoto [a], T. Saito [a], S. Fujibayashi [a], M. Neo [a], S. Yamaguchi [b], T. Kizuki [b], T. Matsushita [b], M. Niinomi [c], T. Kokubo [b], T. Nakamura [a]

[a] Department of Orthopaedic Surgery, Graduate School of Medicine, Kyoto University, Shogoin, Kawahara-cho 54, Sakyo-ku, Kyoto 606-8507, Japan
[b] Department of Biomedical Sciences, College of Life and Health Sciences, Chubu University, 1200 Matsumoto-cho, Kasugai, Aichi 487-8501, Japan
[c] Department of Biomaterials Science, Institute for Materials Research, Tohoku University, 2-1-1 Katahira, Aoba-ku, Sendai 980-8577, Japan

ARTICLE INFO

Article history:
Received 2 July 2010
Received in revised form 17 September 2010
Accepted 20 September 2010
Available online 29 September 2010

Keywords:
Titanium alloy
Bioactive treatment
Apatite
Bone bonding
In vivo

ABSTRACT

Ti15Zr4Nb4Ta and Ti29Nb13Ta4.6Zr, which do not contain the potentially cytotoxic elements V and Al, represent a new generation of alloys with improved corrosion resistance, mechanical properties, and cytocompatibility. Recently it has become possible for the apatite forming ability of these alloys to be ascertained by treatment with alkali, $CaCl_2$, heat, and water (ACaHW). In order to confirm the actual in vivo bioactivity of commercially pure titanium (cp-Ti) and these alloys after subjecting them to ACaHW treatment at different temperatures, the bone bonding strength of implants made from these materials was evaluated. The failure load between implant and bone was measured for treated and untreated plates at 4, 8, 16, and 26 weeks after implantation in rabbit tibia. The untreated implants showed almost no bonding, whereas all treated implants showed successful bonding by 4 weeks, and the failure load subsequently increased with time. This suggests that a simple and economical ACaHW treatment could successfully be used to impart bone bonding bioactivity to Ti metal and Ti–Zr–Nb–Ta alloys in vivo. In particular, implants heat treated at 700 °C exhibited significantly greater bone bonding strength, as well as augmented in vitro apatite formation, in comparison with those treated at 600 °C. Thus, with this improved bioactive treatment process these advantageous Ti–Zr–Nb–Ta alloys can serve as useful candidates for orthopedic devices.

1. Introduction

Titanium (Ti) and its alloys are the most popular materials for orthopedic and dental implants because of their superior biocompatibility, excellent corrosion resistance, and good mechanical properties. However, they are essentially bioinert materials that, after implantation in the living body, are merely encapsulated by fibrous tissue that isolates them from the surrounding tissue. On the other hand, orthopedic load-bearing devices such as total hip prostheses require direct bonding between living bone and the implant. Hence, various methods have been developed to promote bone in-growth and implant fixation for Ti and its alloys [1,2], including physical modification of the implant design, modification of the surface topography, and chemical modification of the material composition and structure. Among these methods, plasma sprayed hydroxyapatite coating is one of the most extensively investigated methods, and its efficiency has been confirmed by many reports [3,4].

In the past decade we have developed a chemical and heat treatment method to produce bioactive Ti [5–7]. This method can be used to create a long-lasting bioactive layer on the surface of Ti and its alloys, allowing bonding with living bone via a spontaneously formed apatite layer. In this method the implants are simply immersed in aqueous solutions before heat treatment, and the bonding effects extend homogeneously throughout the irregular structure of the implant. This method is considered superior to the conventional hydroxyapatite plasma spray method, wherein the coating tends to be applied to the most superficial areas, thereby resulting in uneven and inadequate treatment. This alkali and heat treatment was applied to a porous commercially pure Ti (cp-Ti) surface layer on an artificial hip prosthesis made of a Ti6Al2Nb1Ta alloy, and its effectiveness was confirmed in clinical trials in Japan [8]. In fact, this bioactive artificial hip joint was approved for clinical use in 2007 (AHFIX, Japan Medical Materials Co., Japan).

We have also reported that our chemical and heat treatment is effective for Ti alloys (Ti6Al4V, Ti15Mo5Zr3Al, and Ti6Al2Nb1Ta) [9–11]. However, these Ti alloys contain aluminum (Al) and vanadium (V), which are suspected of being cytotoxic [12–14]. In this

* Corresponding author. Tel.: +81 75 751 3365; fax: +81 75 751 8409.
E-mail address: akinobu@kuhp.kyoto-u.ac.jp (A. Fukuda).

1742-7061/$ - see front matter © 2010 Acta Materialia Inc. Published by Elsevier Ltd. All rights reserved.
doi:10.1016/j.actbio.2010.09.026

context, the new generation of Ti alloys without V and Al [14], such as Ti15Zr4Ta4Nb and Ti29Nb13Ta4.6Zr, offers a promising alternative. Ti15Zr4Ta4Nb has been reported to show much better corrosion resistance, mechanical properties, and cytocompatibility than Ti6Al4V [15]; furthermore, Ti29Nb13Ta4.6Zr has been reported to show a lower Young's modulus and cytotoxicity than Ti6Al4V and the same cytotoxicity as cp-Ti [14,16]. Unfortunately, these new generation Ti alloys cannot be endowed with in vitro apatite forming ability by conventional chemical and heat treatment.

Instead, we recently found that Ti15Zr4Ta4Nb and Ti29Nb13-Ta4.6Zr can be endowed with in vitro apatite forming ability by treatment with NaOH, $CaCl_2$, heat, and water (ACaHW). In vitro examination showed faster and greater apatite formation on the obtained calcium-modified titanate surface in simulated body fluid (SBF), with ion concentrations nearly equal to those of human blood plasma [17,18]. In this treatment calcium hydrogen titanate is formed after treatment of the Ti surface with NaOH and $CaCl_2$. Subsequent heat treatment transforms the calcium hydrogen titanate into calcium titanates and rutile [17,19]. The final water treatment causes a remarkable increase in in vitro apatite forming ability on account of the increasing mobility of the Ca^{2+} ions via incorporation of H_3O^+ ions in the calcium titanate [17]. These results lead us to expect superior in vivo bioactivity when the ACaHW treatment is applied [20]. In the present study, to confirm the in vivo bioactivity of ACaHW-treated cp-Ti, Ti15Zr4Ta4Nb, and Ti29Nb13Ta4.6Zr alloys, the biomechanical performance was investigated by histological examination and tensile strength testing using animal models [21].

2. Materials and methods

2.1. Implant preparation

Plates of size $15 \times 10 \times 2$ mm were prepared from cp-Ti (Ti > 99.5 mass%), Ti15Zr4Ta4Nb (Kobe Steel Ltd.; Ti balance, Zr 14.51, Nb 3.83, Ta 3.94, Pd 0.16, O 0.25 mass%), and Ti29Nb13-Ta4.6Zr (Institute for Materials Research, Tohoku University; Ti balance, Nb 28.8, Fe 0.03,Ta 11.7, Zr 4.65, O 0.08, N 0.01, C 0.01 mass%). The plates were polished with a No. 400 diamond plate, then washed with acetone, 2-propanol, and ultrapure water in an ultrasonic cleaner for 30 min each, and finally dried at 40 °C. For bioactivation the plates were first soaked in 10 ml of 5 or 1 M aqueous NaOH solution at 60 °C for 24 h (alkali treatment). After removal from the solution they were gently rinsed with ultrapure water for 30 s and dried at 40 °C. The plates were subsequently soaked in 20 ml of 100 mM $CaCl_2$ solution at 40 °C for 24 h ($CaCl_2$ treatment), and then washed and dried in a similar manner. Next, they were heated to 600 °C (ACaH600 W) or 700 °C (ACaH700 W) at a rate of 5 °C min^{-1} in an electrical furnace in air and kept at that temperature for 1 h, followed by natural cooling. After the heat treatment they were soaked in 20 ml of ultrapure water at 80 °C for 24 h, and then washed and dried (water treatment). The concentrations of NaOH and the temperatures used for the heat treatment are listed in Table 1. In the present study we did not use ACaH600W-treated Ti29Nb13Ta4.6Zr because the Ti29Nb13-Ta4.6Zr alloy had not showed apatite forming ability in SBF on ACaH600W treatment in a preliminary study. Untreated plates were used as controls in the animal experiments. Thus, a total of eight different types of plates were implanted.

Table 1
Conditions of treatment with $CaCl_2$, heat, and water after treatment with NaOH.

	Concentration of NaOH solution (60 °C 24 h)	Heat treatment temperature (1 h)
cp-Ti	5 mol l^{-1}	600 °C
	5 mol l^{-1}	700 °C
Ti15Zr4Ta4Nb	5 mol l^{-1}	600 °C
	5 mol l^{-1}	700 °C
Ti29Nb13Ta4.6Zr	1 mol l^{-1}	700 °C

2.2. Surface analyses

The surfaces of the treated plates were analyzed by field emission scanning electron microscopy (FE-SEM) (S-4300, Hitachi Co., Tokyo, Japan) equipped with an energy dispersive X-ray (EDX) analyzer (EMAX-7000, Horiba Ltd., Kyoto, Japan). The FE-SEM and EDX analyses were carried out at accelerating voltages of 15 and 5 keV, respectively.

2.3. Apatite formation in SBF

The apatite forming abilities of the treated plates were examined by soaking them in 48 ml of SBF with ion concentrations (Na^+ 142.0, K^+ 5.0, Ca^{2+} 2.5, Mg^{2+} 1.5, Cl^- 147.8, HCO_3^- 4.2, HPO_4^{2-} 1.0, and SO_4^{2-} 0.5 mM) nearly equal to those of human blood plasma at 36.5 °C [22]. After soaking for 1 or 3 days the plates were removed, gently rinsed with ultrapure water for 30 s, and dried at 40 °C. Apatite formation on their surfaces was examined by FE-SEM and EDX.

2.4. Animal study

The plates were conventionally sterilized using ethylene oxide gas and implanted into the metaphyses of the tibiae of mature male Japanese white rabbits weighing 2.8–3.5 kg. The surgical methods used have been described previously [5,10,21,23]. Briefly, the rabbits were anesthetized with an intravenous injection of sodium pentobarbital (0.5 ml kg^{-1}), an intramuscular injection of ketamine hydrochloride (10 mg kg^{-1}), and local administration of a solution of 1% lidocaine. A 3 cm long longitudinal skin incision was made on the medial side of the knee and the fascia and periosteum were incised and retracted to expose the tibial cortex. Using a dental burr, a 16×2 mm^2 hole was made from the medial to the lateral cortex running parallel to the longitudinal axis of the tibial metaphyses, as shown in Fig. 1A. After irrigating the hole with saline, the plates were implanted in the frontal direction, perforating the tibia and protruding from the medial to lateral cortex. The fascia and skin were closed in layers and the same surgical procedures were performed bilaterally.

The animals were housed individually in standard rabbit cages and fed standard rabbit food and water ad libitum. Each rabbit was killed with an overdose of intravenous sodium pentobarbital at 4, 8, 16, and 26 weeks after implantation; a total of 128 rabbits were used (eight plates of each type). The Kyoto University guidelines for animal experiments were observed in this study.

2.5. Measurement of detachment failure load

After death the segments of the proximal tibial metaphyses containing the implanted plates were harvested and prepared for the detachment tests [21]. All samples were kept moist after harvesting. The bone tissue surrounding the plates was carefully removed on both sides and at the ends using a dental burr to remove periosteal bone growth. Traction was applied vertically to the implant surface employing load test equipment (model 1310VRW, Aikoh Engineering Co. Ltd., Nagoya, Japan) at a crosshead speed of 35 mm min^{-1} (Fig. 1B–D). Specially designed hooks held the bone–plate–bone construct. The detachment failure load was measured when the plate detached from the bone. If the plate detached before the test then the failure load was defined as 0 N.

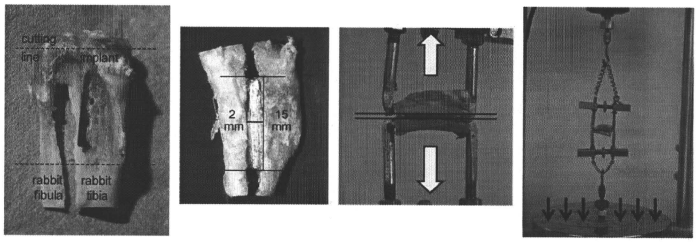

Fig. 1. Photographs of the preparation of rabbit tibia for the detachment test. (A) Insertion of the titanium implant into the tibia (dotted line denotes the cutting line). (B) Detached fragment after cutting the tibia at the proximal and distal ends of the implant. (C) Detachment test. A tensile load is applied by holding the anterior and posterior cortices until detachment. The white arrow indicates the direction of pull. (D) Instron-type autograph. Specially designed hooks held the bone–plate–bone construct. The cross-head speed of the circular disc is 35 mm min^{-1}; the disc moves in the direction of the arrow.

Eight samples were analyzed for each type of implant at each implantation period. All data were recorded as the mean ± standard deviation (SD) and assessed using unpaired one-tailed Student's *t*-test for comparison between untreated and ACaH 700W-treated Ti29Nb13Ta4.6Zr implants at each time point (4, 8, 16, and 26 weeks after implantation), and assessed using one-way analysis of variance (ANOVA) followed by Tukey–Kramer multiple comparison post hoc tests for cp-Ti and Ti15Zr4Ta4Nb at each time point. Differences of $P < 0.05$ were considered statistically significant.

2.6. Histological examination

2.6.1. Surface examination after detachment test

After the detachment tests three samples from each group at each interval after implantation were separated from any soft tissue by soaking in 30% sodium hypochlorite aqueous solution for 3 h. Subsequently they were fixed in 10% phosphate-buffered formalin for 3 days and dehydrated in serial concentrations of ethanol (70, 80, 90, 99, 100, and 100 vol.%) for 1 day each. Then they were soaked in isopentyl acetate solution for 1 day and dried in a critical point drying apparatus (hcp-2, Hitachi Ltd., Tokyo, Japan). The samples were sputter-coated with platinum and palladium for SEM observations (S-4700, Hitachi Ltd., Tokyo, Japan) and coated with carbon for SEM–EDX analyses (EMAX-7000, Horiba Ltd., Kyoto, Japan). The SEM–EDX observations were performed mainly at the sample surface.

2.6.2. Interface examination after detachment test

After the detachment tests five samples from each group at each interval after implantation were fixed in 10% phosphate-buffered formalin for 14 days and dehydrated in serial concentrations of ethanol (70, 80, 90, 99, 100, and 100 vol.%) for 3 days each. Then they were embedded in polyester resin. Sections with thicknesses of 1000 μm were cut using a band saw (BS-3000CP, Exact-Apparatebau, Norderstedt, Germany) positioned perpendicular to the axis of the implant. These sections were polished to a thickness of 30–50 mm using a grinding–sliding machine (Microgrinding MG-4000, Exact-Apparatebau, Norderstedt, Germany) and then stained with Stevenel's blue and Van Gieson's picrofuchsin [24]. A thorough microscopic analysis was performed on histological slides using a transmitted light microscope (model Eclipse 80i, Nikon, Tokyo, Japan) combined with a digital camera (Nikon model DS-5M-L1). Other sections were polished with diamond paper and sputter-coated with carbon for SEM studies.

3. Results

3.1. In vitro evaluation

3.1.1. Surface structures

The EDX results showed that: (1) 3.8–5.3 at.% Na was incorporated on the surface on NaOH treatment; (2) the incorporated Na was completely replaced with Ca on subsequent $CaCl_2$ treatment; (3) the amount of Ca incorporated (4.1–5.9 at.%) remained almost unchanged after subsequent heat and water treatments (3.7–5.2 at.%). Similar tendencies were observed in our previous studies on ACaH600W-treated cp-Ti [19] and Ti15Zr4Nb4Ta [17]. The amount of Ca incorporated did not differ between the ACaH600W- and ACaH700W-treated samples.

Fig. 2 shows FE-SEM photographs of the surfaces of the treated implants. A fine network structure was seen at the nanometer scale on all treated samples, although the alloy plates exhibited a finer network structure than the cp-Ti plate.

3.1.2. Apatite formation

Fig. 3 shows FE-SEM photographs of the surfaces of the treated implants that were soaked in SBF for 1 day. The amount of apatite deposited on the ACaH700W-treated implants increased so that the apatite deposits covered almost the entire surface within 1 day of soaking in SBF. However, the apatite deposits on the surface of the ACaH600W-treated Ti15Zr4Ta4Nb implants only partially covered the surface after 1 day, although they extended to cover the entire surface within 3 days of soaking in SBF.

3.2. In vivo evaluation

All rabbits tolerated the surgical procedure well. None exhibited infection of the surgical site, dislocation of the implants, or adverse reactions such as inflammation or foreign body reactions on or around the implants.

3.2.1. Detachment test (failure load)

Some of the untreated implants were detached from bone prior to testing and were assigned a failure load of 0 N. As seen in Fig. 4, the untreated plates showed a slight increase in failure load throughout the experimental period. In contrast, at all time periods the ACaH700W- and ACaH600W-treated groups both showed significantly higher bonding strength than the untreated groups ($P < 0.001$). Among the cp-Ti and Ti15Zr4Ta4Nb plates the ACaH700W-treated samples showed significantly higher bonding strength than the ACaH600W-treated samples at all time periods.

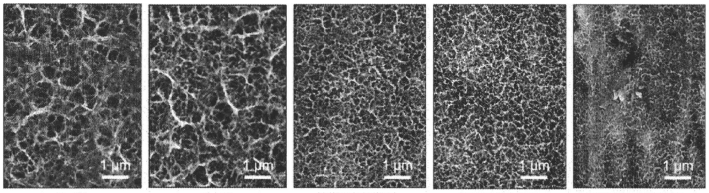

Fig. 2. FE-SEM photographs of the surfaces of the treated implants.

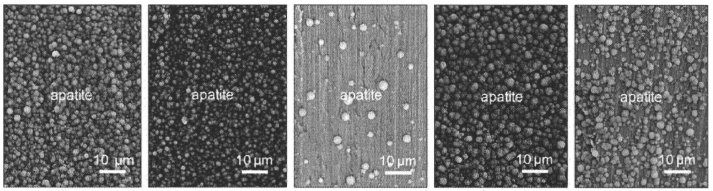

Fig. 3. FE-SEM photographs of the surfaces of the treated implants soaked in SBF for 1 day.

The failure load for all treated groups increased steadily with time. At 4 weeks Ti29Nb13Ta4.6Zr showed a significantly lower bonding strength than cp-Ti and Ti15Zr4Ta4Nb after ACaH700W treatment. Furthermore, from 8 to 26 weeks cp-Ti showed a significantly higher bonding strength than the others after ACaH700W treatment.

3.2.2. Histological examination

3.2.2.1. Surface examination after detachment test. After the detachment tests a bone residue was observed on the intact surface layer of the treated plates in SEM images taken at all time intervals. We could easily distinguish the bony area from the bare metal surface because the average Ca:P ratio in the bony area was 1.66 according to SEM–EDX analysis. In the images taken at 4 weeks there was little bone residue on all untreated plates. In addition, the untreated plates showed almost no increase in bone residue throughout the experimental period. In contrast, some bone residue was observed on the treated plates at 4 weeks, and the amount of residue increased with time. Mature bone was well integrated on the treated plates at all time periods. No significant difference was observed among the ACaH600W- and ACaH700W-treated samples. At 26 weeks, we observed abundant integration of mature bone on the entire treated plate, no surface breakage, and a rupture surface on the bone side for all samples (Fig. 5). Consistent with this finding, in the observations of the bony surface after the detachment testTi was not observed and was not detected by EDX in any sample, indicating that the treated surface structure is sufficiently strong.

3.2.2.2. Interface examination. No inflammatory reactions or adverse effects were observed at the bone–implant interface in all samples subjected to SEM imaging (backscattered mode) and surface staining with Stevenel's blue and Van Gieson's picrofuchsin.

1. At 4 weeks in the untreated group, although immature bone approached the implant, it did not directly bond with the implant, thereby giving rise to a gap between the implant and bone (Fig. 6A). The treated samples, however, all exhibited direct bone–implant bonding, at least partially. However, the bone at the interface was not completely mature in all the implants because of the absence of a laminar structure (Fig. 6). In the stained untreated implant group (Fig. 7A) a little bone formation was found in a transverse direction; the observed bone tissue was of an irregular form without a parallel fibered pattern. In the treated alloy implants newly formed bone bridged the gap, but was coarse and irregular (Fig. 7B, 7C, 7E and 7F). The ACaH700 W-treated cp-Ti implants (Fig. 7D), however, exhibited a bone–Ti interface relatively filled with parallel fibered lamellar bone and bone marrow. Furthermore, the ACaH700W-treated cp-Ti plates had an unclear boundary between new bone and original bone, which indicated bone maturity.
2. At 8 weeks the untreated plates still had a thin layer of intervening fibrous tissue at the interface. However, the treated plates exhibited cortical bone that seemed to extend over the plate. The contact length between cortical bone and implant was wider than that at 4 weeks. Almost complete direct bone bonding was observed in all treated implants.
3. At 16 and 26 weeks the untreated plates still had a thin fibrous tissue layer at the interface or only made partial direct contact with bone (Fig. 8A). Some untreated implants became detached from the bone during cutting, grinding, and staining, which indicated relatively weak bonding. In contrast, the treated samples showed direct bonding with bone and no intervening soft tissue. In particular, the ACaH700W-treated samples exhibited new bone of such maturity that the new bone was undistinguishable from the original bone (Fig. 8D–F), although this was not the case with the ACaH600W-treated plates (Fig. 8B

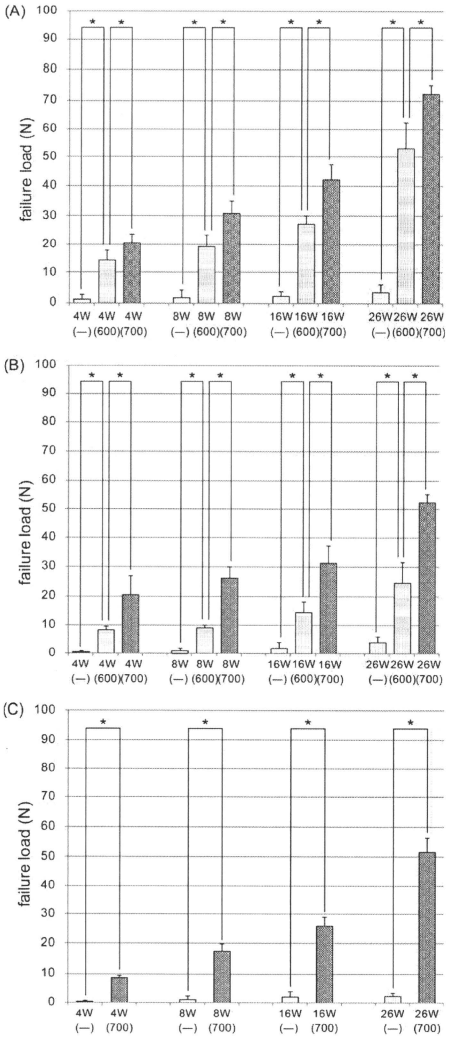

Fig. 4. The results of the detachment test. (A) cp-Ti plates. (B) Ti15Zr4Ta4Nb plates. (C) Ti29Nb13Ta4.6Zr plates. –, Untreated plates; 600, ACaH600W treatment; 700, ACaH700W treatment. The error bars represent standard deviations. * A significant difference.

and 8C). Over time the amount of bone directly bonded to the implant increased, and the directly bonded bone matured and was converted to lamellar bone (Fig. 8B–F).

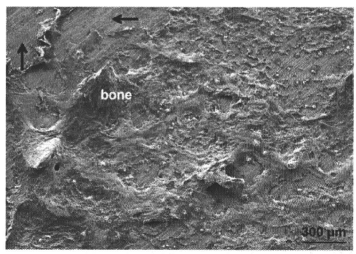

Fig. 5. SEM image of the surface of ACaH700W-treated cp-Ti implants after the detachment test at 26 weeks. Mature bone was well integrated onto the treatment layer. No surface breakage was observed (arrow).

4. Discussion

The results show that all ACaHW-treated implants successfully bonded to bone and retained this bond for up to 26 weeks. In contrast, the untreated implants showed almost no bonding until 8 weeks, and only slight bonding after 16 weeks. Histological examination confirmed that the newly formed bone tissue almost made direct contact with the treated implants as early as 4 weeks after surgery. Conversely, in the untreated implants a layer of fibrous tissue existed at the bone–implant interface 8 weeks after surgery, and bone tissue made only partial contact with the implant at 16 and 26 weeks. These results confirm that ACaHW treatment enhanced bone bonding.

In the present study, cp-Ti showed a relatively higher bonding strength than Ti alloys after ACaHW treatment. The reasons for the differences in bonding strength between ACaHW-treated cp-Ti and Ti alloys are not clear. The bonding strength of the treated substrate is influenced by many factors, such as strength of the substrate and thickness and strength of the treated layers [25]. In general, a thicker calcium titanate layer causes earlier apatite formation and combines with bone earlier than a thin calcium titanate layer. The thickness of the treated layer on cp-Ti and Ti–Zr–Nb–Ta alloys are reported as approximately 1 and 0.5 μm, respectively [17]. This difference may have more impact on the bonding strength than the strength of the substrate.

Ti15Zr4Nb4Ta and Ti29Nb13Ta4.6Zr have been reported to show better biocompatibility than Ti6Al4V [14,16,26,27]. Furthermore, although living bone seems to come close to the surface of these alloys, these bioinert materials do not exhibit osteoconductivity. Recently many researchers have attempted to make these alloys more bioactive, and a few have succeeded [1,2]. Sugino demonstrated apatite formation in vitro on Ti15Zr4Nb4Ta implants subjected to thermal oxidation at 500 °C after machining macrogrooves with widths of 500 μm on the implant surface [1]. Kasuga reported a method for applying a coating of bioactive calcium phosphate invert glass on Ti29Nb13Ta4.6Zr, and showed that the tensile bond between the substrate and coating layer was of high strength [2]. However, these methods cannot be used to treat the entire surface of complex porous implants because of limited apatite formation in the internal surfaces of microgrooves [1] and difficulties encountered with uniform entry of the pulverized glass slurry into the complex microstructure due to its viscous nature [2]. In contrast, our simple method that involves chemical and heat treatment using aqueous solutions and subsequent heat treatment can be used to uniformly treat the entire surface of porous implants having any type of complicated structure. However, our

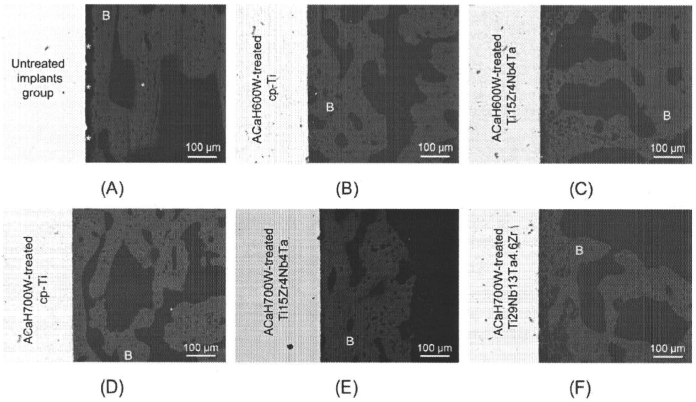

Fig. 6. SEM image (obtained in backscattered mode) of the implant–bone interface at 4 weeks. (A) Untreated implant group. Although immature bone approached the implant, it did not directly bond with the implant, giving rise to a gap (white asterisks) between the implant and the bone. (B) ACaH600W-treated cp-Ti plates. (C) ACaH600W-treated Ti15Zr4Nb4Ta plates. (D) ACaH700W-treated cp-Ti plates. (E) ACaH700W-treated Ti15Zr4Nb4Ta plates. (F) ACaH700W-treated Ti29Nb13Ta4.6Zr plates. Direct bonding between bone and implant was observed for all treated implants. The contact area was comparatively large (D, E) and the new bone was relatively mature and dense. B, bone.

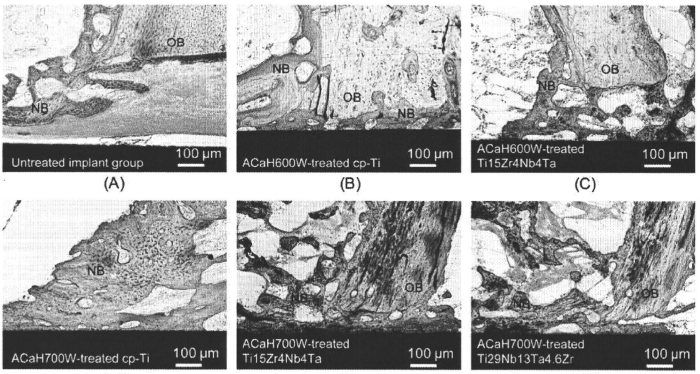

Fig. 7. Surface staining of the bone–implant interface with Stevenel's blue and Van Gieson's picrofuchsin at 4 weeks. (A) Untreated implant group. (B) ACaH600W-treated cp-Ti plates. (C) ACaH600W-treated Ti15Zr4Nb4Ta plates. (D) ACaH700W-treated cp-Ti plates. (E) ACaH700W-treated Ti15Zr4Nb4Ta plates. (F) ACaH700W-treated Ti29Nb13Ta4.6Zr plates. Both the treated and untreated implant groups showed coarse bone formation on the implant. The treated implants (B–F) showed partial direct bone bonding, whereas the untreated implant (A) showed a thick layer of intervening fibrous tissue. The ACaH700W-treated cp-Ti plates (D) had an unclear boundary between the new bone and original bone, which indicated bone maturity. OB, original bone; NB, new bone.

conventional alkali and heat treatment, although successful with Al- and V-containing Ti alloys (Ti6Al4V, Ti15Mo5Zr3Al, and Ti6Al2Nb1Ta) [9–11], was ineffective with Ti15Zr4Nb4Ta and Ti29Nb13Ta4.6Zr.

The increased apatite formation after the NaOH and heat treatments is attributed to the formation of sodium titanate on the surface. In SBF sodium titanate releases Na^+ ions via exchange with H_3O^+ ions to form Ti–OH groups on the surface, which induce apatite formation, as earlier described for NaOH- and heat-treated Ti metal [28,29]. However, Ti containing Ca^{2+} ions instead of Na^+ ions on its surface is expected to exhibit higher apatite formation, since the released Ca^{2+} ions more effectively increase the ionic activity product of the apatite in the surrounding body fluids [30]. In fact, several studies have investigated the incorporation of Ca^{2+} ions onto Ti surfaces [31–33]. However, the techniques mentioned in these studies require expensive specialized apparatus for ion implantation [32] or a specialized high pressure apparatus operating in an aqueous environment at high temperatures for application to medical devices [31,33]. We recently ascertained the in vitro apatite forming ability of cp-Ti, Ti15Zr4Nb4Ta, and

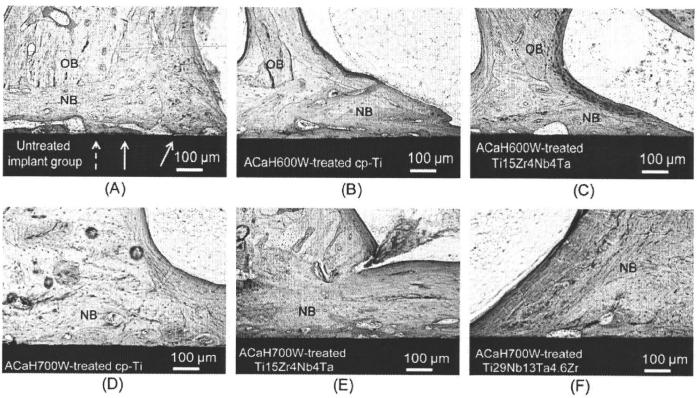

Fig. 8. Surface staining of the bone–implant interface with Stevenel's blue and Van Gieson's picrofuchsin at 16 weeks. (A) Untreated implant group. (B) ACaH600W-treated cp-Ti plates. (C) ACaH600W-treated Ti15Zr4Nb4Ta plates. (D) ACaH700W-treated cp-Ti plates. (E) ACaH700W-treated Ti15Zr4Nb4Ta plates. (F) ACaH700W-treated Ti29Nb13Ta4.6Zr plates. Both the treated and untreated implant groups showed mature bone on the implant. The treated implants (B–F) showed almost complete direct bone bonding, whereas the untreated implant (A) showed a thin layer of intervening fibrous tissue (white arrow) and only partial direct bone bonding (dotted white arrow). The ACaH700W-treated samples exhibited new bone of such maturity that the new bone was undistinguishable from the original bone (D–F), although this was not the case with the ACaH600W-treated plates (B, C). OB, original bone; NB, new bone.

Ti29Nb13Ta4.6Zr alloy implants by using simple and economical ACaHW treatments [17–19]. Furthermore, in the present study an in vivo bone bonding ability was confirmed. The mechanisms of apatite formation following ACaHW treatment are interpreted in terms of surface structural changes as follows. The apatite forming ability increased after $CaCl_2$ treatment following NaOH treatment, although this ability is lost after heat treatment to strengthen the treated layer due to the reduced mobility of Ca^{2+} ions in calcium titanate [17]. This problem is resolved by the subsequent water treatment, which contributes to increased mobility of the Ca^{2+} ions in calcium titanate by incorporation of H_3O^+ ions [17].

We previously reported that sodium removal through hot water immersion in the course of alkali and heat treatment considerably enhanced the apatite forming ability of Ti in SBF. Sodium removal enhanced the bone bonding strength of Ti subjected to alkali and heat treatment at 4 and 8 weeks post-operative, however, the failure loads of the implants subjected to sodium-free alkali and heat treatment decreased after 16 weeks implantation because the treated layer flaked off [5]. On the other hand, the failure loads in the present study did not decrease and no flaking of the treated layer was observed by SEM through to the end. We considered that the stability of the ACaHW-treated layer was confirmed by these results.

In comparison with the case of heat treatment at 600 °C, heat treatment at 700 °C led to a significant improvement in apatite formation in SBF and tensile strength in vivo. However, the EDX results were not significantly different. In the detachment test all treated specimens ruptured on the bone side. Hence, we consider that the differences in failure load between samples subjected to ACaH600W and ACaH700W treatment stem from bone maturity and adhesion based on the histological findings. In other words, the increase in heat treatment temperature to 700 °C increased the extent of bone formation around the implant.

In general, the apatite forming ability of Ti metal subjected to alkali and heat treatment was liable to decrease when the treated Ti metal was stored in a humid environment for a long period of time, because of the release of Na^+ ions from the sodium titanate. However, it is reported that the apatite forming ability of ACaHW-treated Ti metal did not decrease, even when the treated Ti metal was kept in a humid environment [19]; this finding can be attributed to the low mobility of Ca^{2+} ions compared with Na^+ ions in the titanate.

Thus, from an overall perspective, it is expected that when Ti15Zr4Ta4Nb and Ti29Nb13Ta4.6Zr alloys with superior biocompatibility and mechanical properties are endowed with bioactivity and stability through ACaHW treatment, the treated alloys will be useful in developing novel orthopedic implants that function under loaded conditions, such as cementless joint replacement implants, external fixation pins, and spinal fusion implants.

5. Conclusions

Commercially pure Ti and its Zr-, Nb-, and Ta-containing alloys (without V and Al), namely Ti15Zr4Ta4Nb and Ti29Nb13Ta4.6Zr, exhibit enhanced apatite formation in vitro and bone bonding in vivo after alkali, $CaCl_2$, heat, and water treatment. In particular, implants heat treated at 700 °C have significantly augmented apatite formation in SBF and stronger bone bonding in vivo. The present results suggest that these treated Ti alloys may be useful to develop novel orthopedic implants that function under loaded conditions, because of their superior mechanical properties and excellent bioactivity and cytocompatibility.

Acknowledgements

This work was supported by the Translational Research Promotion Project as part of the Health Assurance Program of the New Energy and Industrial Technology Development Organization (NEDO). We thank Dr. Yoshimitsu Okazaki for supplying the alloy used in the study.

Appendix Appendix. A. Figures with essential colour discrimination

Certain figures in this article, particularly Figs. 1, 7, and 8 are difficult to interpret in black and white. The full colour images

can be found in the on-line version, at doi:10.1016/j.actbio.2010.09.026.

References

[1] Sugino A, Ohtsuki C, Tsuru K, Hayakawa S, Nakano T, Okazaki Y, et al. Effect of spatial design and thermal oxidation on apatite formation on Ti–15Zr–4Ta–4Nb alloy. Acta Biomater 2009;5:298–304.

[2] Kasuga T, Nogami M, Niinomi M, Hattori T. Bioactive calcium phosphate invert glass-ceramic coating on beta-type Ti–29Nb–13Ta–4.6Zr alloy. Biomaterials 2003;24:283–90.

[3] De Groot K, Geesink R, Klein C, Serekian R. Plasma sprayed coatings of hydroxyapatite. J Biomed Mater Res 1987;21:1375–81.

[4] Klein CP, Patka P, van der Lubbe HB, Wolke JG, de Groot K. Plasma-sprayed coatings of tetracalciumphosphate, hydroxyl-apatite, and alpha-TCP on titanium alloy: an interface study. J Biomed Mater Res 1991;25:53–65.

[5] Fujibayashi S, Nakamura T, Nishiguchi S, Tamura J, Uchida M, Kim HM, et al. Bioactive titanium: effect of sodium removal on the bone-bonding ability of bioactive titanium prepared by alkali and heat treatment. J Biomed Mater Res 2001;56:562–70.

[6] Takemoto M, Fujibayashi S, Neo M, Suzuki J, Kokubo T, Nakamura T. Mechanical properties and osteoconductivity of porous bioactive titanium. Biomaterials 2005;26:6014–23.

[7] Takemoto M, Fujibayashi S, Neo M, Suzuki J, Matsushita T, Kokubo T, et al. Osteoinductive porous titanium implants: effect of sodium removal by dilute HCl treatment. Biomaterials 2006;27:2682–91.

[8] Kawanabe K, Ise K, Goto K, Akiyama H, Nakamura T, Kaneuji A, et al. A new cementless total hip arthroplasty with bioactive titanium porous-coating by alkaline and heat treatment: average 4.8-year results. J Biomed Mater Res B Appl Biomater 2009;90:476–81.

[9] Kim HM, Miyaji F, Kokubo T, Nakamura T. Preparation of bioactive Ti and its alloys via simple chemical surface treatment. J Biomed Mater Res 1996;32:409–17.

[10] Nishiguchi S, Kato H, Fujita H, Kim HM, Miyaji F, Kokubo T, et al. Enhancement of bone-bonding strengths of titanium alloy implants by alkali and heat treatments. J Biomed Mater Res 1999;48:689–96.

[11] Kim HM, Takadama H, Kokubo T, Nishiguchi S, Nakamura T. Formation of a bioactive graded surface structure on Ti–15Mo–5Zr–3Al alloy by chemical treatment. Biomaterials 2000;21:353–8.

[12] Steinemann S. Corrosion of Surgical Implants – In Vivo and In Vitro Tests. New York: Wiley; 1980.

[13] Hallab NJ, Vermes C, Messina C, Roebuck KA, Glant TT, Jacobs JJ. Concentration- and composition-dependent effects of metal ions on human MG-63 osteoblasts. J Biomed Mater Res 2002;60:420–33.

[14] Niinomi M. Metallic biomaterials. J Artif Organs 2008;11:105–10.

[15] Okazaki Y, Rao S, Ito Y, Tateishi T. Corrosion resistance, mechanical properties, corrosion fatigue strength and cytocompatibility of new Ti alloys without Al and V. Biomaterials 1998;19:1197–215.

[16] Niinomi M. Fatigue performance and cyto-toxicity of low rigidity titanium alloy, Ti–29Nb–13Ta–4.6Zr. Biomaterials 2003;24:2673–83.

[17] Yamaguchi S, Takadama H, Matsushita T, Nakamura T, Kokubo T. Apatite-forming ability of Ti–15Zr–4Nb–4Ta alloy induced by calcium solution treatment. J Mater Sci Mater Med, 2009.

[18] Yamaguchi S, Kizuki T, Takadama H, Matsushita T, Kokubo T, Fukuda A, et al. Preparation of Bioactive Ti–Nb–Ta–Zr Alloy by Chemical Treatment. Aichi: Japanese Society of Orthopaedic Ceramic Implants; 2009.

[19] Kizuki T, Takadama H, Matsushita T, Nakamura T, Kokubo T. Preparation of bioactive Ti metal surface enriched with calcium ions by chemical treatment. Acta Biomater 2010.

[20] Fujibayashi S, Neo M, Kim HM, Kokubo T, Nakamura T. A comparative study between in vivo bone ingrowth and in vitro apatite formation on Na_2O–CaO–SiO_2 glasses. Biomaterials 2003;24:1349–56.

[21] Nakamura T, Yamamuro T, Higashi S, Kokubo T, Itoo S. A new glass-ceramic for bone replacement: evaluation of its bonding to bone tissue. J Biomed Mater Res 1985;19:685–98.

[22] Kokubo T, Takadama H. How useful is SBF in predicting in vivo bone bioactivity? Biomaterials 2006;27:2907–15.

[23] Onishi E, Fujibayashi S, Takemoto M, Neo M, Maruyama T, Kokubo T, et al. Enhancement of bone-bonding ability of bioactive titanium by prostaglandin E_2 receptor selective agonist. Biomaterials 2008;29:877–83.

[24] Maniatopoulos C, Rodriguez A, Deporter DA, Melcher AH. An improved method for preparing histological sections of metallic implants. Int J Oral Maxillofac Implants 1986;1:31–7.

[25] Takemoto M, Nakamura T. Osteoconduction and its evaluation. In: Kokubo T, editor. Bioceramics and their Clinical Applications. Cambridge: Woodhead Publishing; 2008. p. 183–98.

[26] Okazaki Y, Nishimura E, Nakada H, Kobayashi K. Surface analysis of Ti–15Zr–4Ta alloy after implantation in rat tibia. Biomaterials 2001;22:599–607.

[27] Sumitomo N, Noritake K, Hattori T, Morikawa K, Niwa S, Sato K, et al. Experiment study on fracture fixation with low rigidity titanium alloy: plate fixation of tibia fracture model in rabbit. J Mater Sci Mater Med 2008;19:1581–6.

[28] Takadama H, Kim HM, Kokubo T, Nakamura T. An X-ray photoelectron spectroscopy study of the process of apatite formation on bioactive titanium metal. J Biomed Mater Res 2001;55:185–93.

[29] Takadama H, Kim HM, Kokubo T, Nakamura T. TEM–EDX study of mechanism of bonelike apatite formation on bioactive titanium metal in simulated body fluid. J Biomed Mater Res 2001;57:441–8.

[30] Ohtsuki C, Kokubo T, Yamamuro T. Mechanism of apatite formation on CaO–SiO_2–P_2O_5 glasses in a simulated body fluid. J Non-Cryst Solids 1992;143:84–92.

[31] Chen XB, Li YC, Du Plessis J, Hodgson PD, Wen C. Influence of calcium ion deposition on apatite-inducing ability of porous titanium for biomedical applications. Acta Biomater 2009;5:1808–20.

[32] Nayab SN, Jones FH, Olsen I. Effects of calcium ion implantation on human bone cell interaction with titanium. Biomaterials 2005;26:4717–27.

[33] Park JW, Park KB, Suh JY. Effects of calcium ion incorporation on bone healing of Ti6Al4V alloy implants in rabbit tibiae. Biomaterials 2007;28:3306–13.

Acta Biomaterialia 7 (2011) 1398–1406

Contents lists available at ScienceDirect

Acta Biomaterialia

journal homepage: www.elsevier.com/locate/actabiomat

Bioactive Ti metal analogous to human cancellous bone: Fabrication by selective laser melting and chemical treatments

Deepak K. Pattanayak [a,*,1], A. Fukuda [b,1], T. Matsushita [a], M. Takemoto [b], S. Fujibayashi [b], K. Sasaki [c], N. Nishida [c], T. Nakamura [b], T. Kokubo [a]

[a] Department of Biomedical Sciences, College of Life and Health Sciences, Chubu University, Japan
[b] Department of Orthopaedic Surgery, Graduate School of Medicine, Kyoto University, Japan
[c] Sagawa Printing Co. Ltd., Kyoto, Japan

ARTICLE INFO

Article history:
Received 10 August 2010
Received in revised form 22 September 2010
Accepted 24 September 2010
Available online 29 September 2010

Keywords:
Selective laser melting
Porous titanium
Chemical treatment
Compressive strength
In vitro and in vivo studies

ABSTRACT

Selective laser melting (SLM) is a useful technique for preparing three-dimensional porous bodies with complicated internal structures directly from titanium (Ti) powders without any intermediate processing steps, with the products being expected to be useful as a bone substitute. In this study the necessary SLM processing conditions to obtain a dense product, such as the laser power, scanning speed, and hatching pattern, were investigated using a Ti powder of less than 45 μm particle size. The results show that a fully dense plate thinner than 1.8 mm was obtained when the laser power to scanning speed ratio was greater than 0.5 and the hatch spacing was less than the laser diameter, with a 30 μm thick powder layer. Porous Ti metals with structures analogous to human cancellous bone were fabricated and the compressive strength measured. The compressive strength was in the range 35–120 MPa when the porosity was in the range 75–55%. Porous Ti metals fabricated by SLM were heat-treated at 1300 °C for 1 h in an argon gas atmosphere to smooth the surface. Such prepared specimens were subjected to NaOH, HCl, and heat treatment to provide bioactivity. Field emission scanning electron micrographs showed that fine networks of titanium oxide were formed over the whole surface of the porous body. These treated porous bodies formed bone-like apatite on their surfaces in a simulated body fluid within 3 days. In vivo studies showed that new bone penetrated into the pores and directly bonded to the walls within 12 weeks after implantation into the femur of Japanese white rabbits. The percentage bone affinity indices of the chemical- and heat-treated porous bodies were significantly higher than that of untreated implants.

1. Introduction

Titanium (Ti) metal and its alloys are widely used for various implants in the orthopedic and dental fields, because of their good biocompatibility and high mechanical strength. However, their elastic moduli are higher than that of living bone and, hence, they are liable to induce bone resorption due to stress shielding. If a considerable amount of interconnected pores are introduced into them, their elastic moduli decrease to the level of cancellous bone. In addition, bone tissue can grow into the pores to integrate with them. Therefore, various methods have been developed for producing porous bodies of Ti metal and its alloys [1]. Among them, the most common method is sintering of metal powders with added volatile materials [2,3]. Recently, selective laser sintering (SLS) [4–10], selective laser melting (SLM) or direct laser forming (DLF) [11–18] and selective electron beam melting (SEBM) [19] processes have been applied to produce porous bone substitutes. The SLS process produces a porous body by partial sintering of metal powders. On the other hand, in the DLF/SLM and SEBM processes the metal powders are completely melted and fused by a laser or electron beam, respectively, resulting in a porous body within a short period of time [13,19]. Attempts have been made to produce various kinds of porous Ti metal with simple interconnected porous structures by the SLM process [11,12,17]. However, preparation of porous Ti metal with a structure analogous to human cancellous bone has not been reported.

In the SLM process three-dimensional (3D) structures can be prepared from metal powders without any additional processing steps. However, in order to obtain a defect-free specimen, it is essential to optimize the processing parameters of the SLM technique, i.e. laser power, scanning speed, hatching pattern, etc.

Although Ti metal and titanium alloys are biocompatible, they do not bond to living bone directly when implanted into a bone defect [20]. However, Ti metal subjected to NaOH and heat treatments to form sodium titanate on its surface spontaneously bonds

* Corresponding author. Tel.: +81 568 51 9731; fax: +81 568 51 5370.
E-mail addresses: deepak@isc.chubu.ac.jp, deepak_pattanayak@rediffmail.com (D.K. Pattanayak).
[1] The first two authors contributed equally to this study.

1742-7061/$ - see front matter © 2010 Acta Materialia Inc. Published by Elsevier Ltd. All rights reserved.
doi:10.1016/j.actbio.2010.09.034

Table 1
Chemical composition of the titanium powder (mass%).

O	Fe	H	C	N	Ni	Cr	Si	Ti
0.121	0.029	0.005	0.010	0.006	0.003	0.003	0.001	Balance

to living bone through an apatite layer formed on its surface in the living body [21–23]. This bioactive Ti metal has been applied to an artificial hip joint, and its effectiveness has already been confirmed in clinical trials [24]. This bioactive artificial hip joint (AHFIX, Japan Medical Materials Co., Japan) has been approved for clinical use in Japan since 2007.

Ti metal subjected to NaOH, HCl, and heat treatments to form Na-free titanium oxide on its surface has also been found to form a bone-like apatite layer in a simulated body fluid (SBF) [25] and to exhibit osteoconductivity as well as osteoinductivity [26–28].

In the present study plate specimens were first fabricated by the SLM process using commercially pure Ti powders. The effect of processing parameters such as power, scanning speed, and scanning pattern of the laser beam on the density of the plate specimens was investigated. Porous Ti metal with a structure analogous to human cancellous bone was prepared using the optimum operating conditions and its compressive strength measured. It was subjected to NaOH, HCl, and heat treatment for bioactivation and its apatite-forming ability in SBF and bone-bonding abilities in rabbit femurs examined.

2. Materials and methods

2.1. Materials

A gas atomized commercially pure Ti metal powder (grade 2, Osaka Titanium Technologies Co. Ltd., Japan) with a particle size of <45 μm was used as the starting powder. Its chemical composition is given in Table 1.

2.2. Selective laser melting

2.2.1. Determination of optimum conditions

Fig. 1 shows schematically the selective laser melting process. In the present experiment an SLM system (EOSINT-M270, Electro Optical Systems GmbH, Germany) was used. A 3D model was designed by computer-aided design (CAD) software (Magics, Materialise, Belgium). This 3D model was horizontally sliced into many thin layers of two-dimensional images. In this system a Yb fiber laser beam of nominal diameter 100 μm and with a maximum power of 200 W moves at a maximum speed of 7000 mm s^{-1} in an argon gas environment. According to the data for the slices provided by the computer the laser beam scans the Ti metal powder layer to selectively melt it, producing the prescribed two-dimensional metallic structures. In the next step the platform moves vertically downwards, allowing the deposition of an unfused powder layer at a 30 μm interval. Again, the laser beam selectively melts the second layer over the first layer, and this process is continued repeatedly to construct the final 3D metallic structure. The manufactured specimen was removed from the platform. The specimens were cleaned ultrasonically using acetone, 2-propanol, and ultrapure water for 30 min each to remove residual unfused powder sticking to the walls of the specimen.

Fig. 2 shows the standard scanning strategy for the fabrication of the specimen using a boundary contour beam of 58.5 W power followed by a hatch beam of 117 W, with a hatch space of 180 μm and a hatch offset of 20 μm. In each subsequent layer the hatch lines are rotated with respect to the previous layer by 66.7° to melt the powder completely. In order to investigate the effect of energy density on the density of the fabricated specimen, the laser power was varied from 90 to 180 W at a constant scanning speed of 225 mm s^{-1} and constant powder layer of 30 μm thickness, so that the power to speed ratio (P/V) was in the range 0.3–0.8 W mm^{-1} s^{-1}. Specimens of $9 \times 9 \times 9$ mm^3 size were formed at different P/V ratios. Their densities were measured using Archimedes' principle. In addition to the above, $9 \times 9 \times t$ mm^3 specimens of different thicknesses (t) were formed by using a hatch space of 90 and 180 μm, and their densities were also measured using the same technique.

2.2.2. Fabrication of a porous structure analogous to human cancellous bone

Porous Ti metals with a structure similar to that of human cancellous bone with different porosities were fabricated using the optimized processing conditions of laser power, scanning speed, and hatching pattern. In this process micro-CT images of the structure of cancellous bone were stored in a computer and modified a little due to certain limitations of this method. For example, wall thicknesses of less than 200 μm are difficult to process and, hence, the wall thickness was increased to more than 300 μm. In this process specimens were always prepared from the bottom to the top.

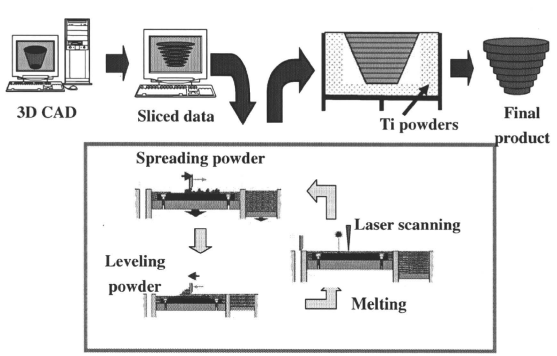

Fig. 1. Schematic representation of the SLM process.

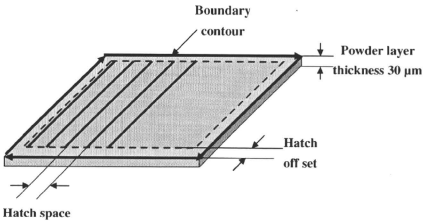

Fig. 2. Schematic representation of various operating parameters which affect the product density in the SLM process.

Therefore, a foothold was provided for the bone structure. Then the image was sliced at 30 μm intervals. Porous structures were fabricated using Ti metal powder according to the sliced data by the method described in Section 2.2.1. Fig. 3a shows a CT image of the cancellous bone structure of a 53-year-old male, while (i) is a porous body produced by multiple stacking of the unit structure in (a). Fig. 3b shows a CT image of the cancellous bone of a 48-year-old female, while (ii) is a porous body produced from (b). Fig. 3ii is referred to as CBS in subsequent studies. Fig. 3c shows a hollow cubic unit cell and its stacking, while (iii) is a porous body produced from (c). This is referred to as IPS in subsequent studies. These three types of specimens were produced with different porosities by changing the wall thickness. Cancellous bone structures consist of interconnected pores of different sizes ranging from 500 μm to 2 mm (Fig. 3i and ii), while the cubic structure has interconnected pores in the range 400–800 μm (Fig. 3iii). These specimens were washed with acetone, 2-propanol, and ultrapure water for 30 min each in an ultrasonic cleaner and then dried in an oven at 40 °C overnight. Later, the CBS and IPS specimens were subjected to heat treatment at 1300 °C in an argon gas atmosphere to smooth the surface.

2.3. Chemical and heat treatment for bioactivity

The porous Ti metal specimens CBS and IPS were first soaked in 5 M NaOH solution at 60 °C for 24 h and then soaked in 0.5 mM HCl solution at 40 °C for 3 h to bioactivate them. A continuous-flow method was used to treat these specimens to avoid non-uniform chemical treatment inside the pores along the length. Later, these specimens were washed in ultrapure water, dried in an oven at 40 °C overnight and then heated to 600 °C at a rate of 5 °C min^{-1}. The specimens were kept in a Fe–Cr electric furnace under an air atmosphere at 600 °C for 1 h and finally cooled to room temperature naturally in the furnace.

2.4. Analysis of the surface structures and measurement of compressive strength

The surface texture of the porous Ti metal as prepared, in addition to being subsequently subjected to heat treatment at 1300 °C in an argon gas atmosphere, was observed by field emission scanning electron microscopy (FE-SEM) (Hitachi S-4300, Japan). Surface structural changes due to the NaOH, HCl, and heat treatments and subsequent soaking in SBF were also observed by FE-SEM.

The compressive strengths of porous bodies of Ti metal with the different structures shown in Fig. 3i–iii were measured using a universal testing machine (model EHF-LV020K1-010, Shimadzu Corp., Japan) at a cross-head speed of 1 mm min^{-1}.

2.5. Examination of the apatite forming ability in a simulated body fluid (SBF)

Porous Ti metal subjected to chemical and heat treatment was soaked in 30 ml of an acellular SBF with ion concentrations of Na^+ 142.0, K^+ 5.0, Mg^{2+} 1.5, Ca^{2+} 2.5, Cl^-147.8, HCO_3^- 4.2, HPO_4^{2-} 1.0, and SO_4^{2-} 0.5 mM, nearly equal to those of human blood plasma, at 36.5 °C for 3 days. The SBF was prepared by dissolving reagent grade NaCl, $NaHCO_3$, KCl, $K_2HPO_4{\cdot}3H_2O$, $MgCl_2{\cdot}6H_2O$, $CaCl_2$, and Na_2SO_4 (Nacalai Tesque Inc., Kyoto, Japan) in ultrapure

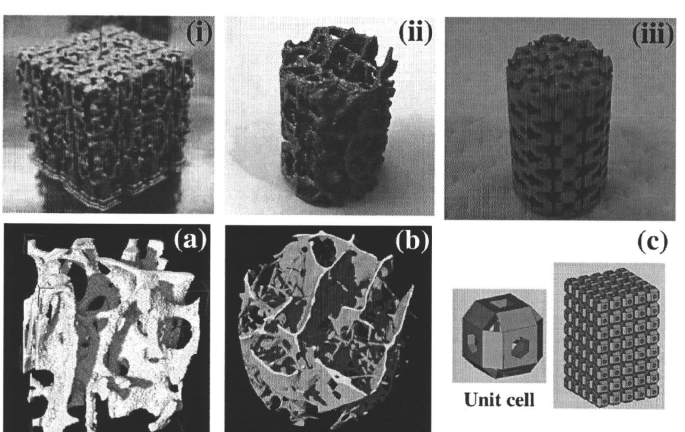

Fig. 3. Titanium porous structure fabricated by SLM (i–iii) based on micro-CT images of human cancellous bones (a, b) and stacked hollow cubes (c). Specimen size: (a) 15 × 15 × 15 mm; (b, c) 6 mm diameter, 10 mm length. Notation: (ii) CBS; (iii) IPS.

water buffered at pH 7.40 with Tris and 1 M HCl (Nacalai Tesque) [29]. After 3 days soaking the specimens were removed from the SBF, gently washed with ultrapure water, and dried at 40 °C in an oven. Apatite formation on the walls was examined by FE-SEM.

2.6. In vivo examination of new bone formation in white rabbits

2.6.1. Animal study

Porous Ti metal specimens of CBS and IPS 6 mm in outer diameter and 15 mm in length, subjected to chemical and heat treatments, were conventionally sterilized using ethylene oxide gas and implanted into the metaphyses of the femoral condyles of mature male Japanese white rabbits weighing 2.8–3.5 kg. The surgical methods used have been described elsewhere [30,31]. Briefly, the rabbits were anesthetized with intravenous injections of sodium pentobarbital (0.5 ml kg^{-1}), an intramuscular injection of ketamine hydrochloride (10 mg kg^{-1}), and local administration of a solution of 1% lidocaine. After shaving, disinfection, and draping, the fascia was split and a 6 mm diameter drill hole was made through the femoral condyles. After irrigating the hole with saline, both kinds of porous Ti metal specimens, CBS and IPS, subjected to chemical and heat treatment, were implanted into the hole. For comparison, untreated samples were also implanted in a similar manner. Surgical procedures were performed bilaterally. Twenty-five rabbits were used for the chemical- and heat-treated implants. At 3, 6, 12, 26, and 52 weeks after implantation five rabbits were killed using an overdose of intravenous sodium pentobarbital, i.e. five chemical- and heat-treated implants and five animals per experimental condition. Ten rabbits were used for the untreated implants. At 12 and 52 weeks after implantation these rabbits were killed in the same way, i.e. five untreated implants and five animals per experimental condition. This animal study was approved by the Animal Research Committee, Graduate School of Medicine, Kyoto University, Japan.

2.6.2. Histological examination

Following death the implant sites were removed and prepared for histology. The specimens were fixed in 10% phosphate-buffered formalin, pH 7.25 for 7 days and dehydrated in serial concentrations of ethanol (70%, 80%, 90%, 99%, 100%, and 100% v/v) for 3 days each. Specimens were then embedded in polyester resin. Thick sections (250 μm) were cut with a band saw (BS-3000CP, EXACT Cutting Systems, Norderstedt, Germany) perpendicular to the axis of the implant and ground to a thickness of 50–60 μm using a grinding–sliding machine (Microgrinding MG-4000, EXACT Cutting Systems). Each section was then stained with Stevenel's blue and Van Gieson's picrofuchsin [32]. A thorough microscopic analysis was performed on histological slides using transmitted light microscopy (model Eclipse 80i, Nikon Co., Japan) combined with a digital camera (model DS-5 M-L1, Nikon Co., Japan).

Other thick sections (500 μm) were cut with a band saw, polished with diamond paper, and a thin layer of carbon applied for observation by SEM.

2.6.3. Histomorphometric examination

The bone affinity index (%) was measured on a personal computer using Adobe Photoshop CS3 and Image J (NIH) for each implant using data provided by light microscopy and fluorescence microscopy. The bone affinity index is defined as the fraction of bone contact over the entire wall of the pores in the implant [26,31,33]. Two sections surrounded with cancellous bone from either the medial or the lateral condyles were examined for each implant. Thus, 10 slices were analyzed for each implantation time.

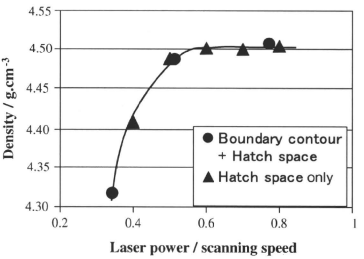

Fig. 4. Variation in density of the solid cubic specimens with change in laser power to scanning speed ratio at a constant powder layer thickness. Specimen size $9 \times 9 \times 9$ mm^3; hatch space 180 μm; scanning speed 225 mm s^{-1}.

2.6.4. Statistical analysis

All data are expressed as means ± standard deviation (SD) and were statistically analyzed using JMP IN 5.1 (SAS Institute, Cary, NC). The unpaired one-tailed Student's *t*-test was used for comparison between the implant (bioactive treated and untreated) at each time point (12 and 52 weeks). One-way ANOVA followed by post hoc tests (Tukey–Kramer multiple comparison tests) were used to analyze temporal bone formation in each implant type. Differences at $P < 0.05$ were considered statistically significant.

3. Results

3.1. Effects of processing parameters on the density of the specimen

Fig. 4 shows the variation in density of specimens with laser power to scanning speed (*P*/*V*) ratio, where specimens were fabricated using a boundary contour followed by a hatch beam with a hatch space of 180 μm. Specimens were also prepared using only a hatch beam with a hatch space of 180 μm. From Fig. 4 we can see that in both cases the density of the specimen was low when the *P*/*V* ratio was <0.5, and reached the theoretical density (4.51 g cm^{-3}) of Ti metal when the P/V ratio was >0.60.

Fig. 5 shows the density of Ti plates of different thicknesses, which were fabricated at two different hatch beam spaces of 90 and 180 μm at a constant *P*/*V* ratio of 0.51. The density was nearly equal to that of the theoretical density when the thickness of the prepared specimen was >1.8 mm, irrespective of the space between the two consecutive hatch beams. A high density was observed for plates with a thickness of <1.8 mm when the hatch beam space was 90 μm. The effect of hatch beam offsets of 0, 10,

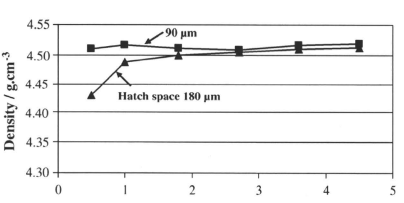

Fig. 5. Effect of hatch space on density of solid specimens of different thicknesses. Specimen size $9 \times 9 \times t$ mm^3, where *t* is the thickness of specimen in mm; scanning speed 225 mm s^{-1}.